Effect of aspect-ratio on vortex distribution and heat transfer in rotating Rayleigh-Bénard convection

J. Overkamp[1], R.J.A.M. Stevens[2,*], Detlef Lohse[2] & Herman J.H. Clercx [1,3]

[1]Department of Physics and J.M. Burgers Center for Fluid Dynamics, Eindhoven University of Technology, P.O. Box 513, 5600 MB Eindhoven, The Netherlands
[2]Department of Science and Technology and J.M. Burgers Center for Fluid Dynamics, University of Twente, P.O Box 217, 7500 AE Enschede, The Netherlands.
[3]Department of Applied Mathematics, University of Twente, P.O Box 217, 7500 AE Enschede, The Netherlands

E-mail: r.j.a.m.stevens@tnw.utwente.nl

Abstract.

Numerical and experimental data for the heat transfer as function of the Rossby number Ro in rotating Rayleigh-Bénard are presented for $Pr = 4.38$ and up to $Ra = 4.52 \times 10^9$. The aspect ratio is varied between $\Gamma = 0.5$ and $\Gamma = 2.0$. Without rotation, where the aspect ratio influences the global flow structure, we see a small aspect-ratio dependence in the Nusselt number. For stronger rotation, i.e. $1/Ro \gg 1/Ro_c$, the heat transport becomes independent of the aspect-ratio. We interpret this finding as follows: In the rotating regime the heat is mainly transported by vertically-aligned vortices. Since these vortices are local, the aspect ratio has a negligible effect on the heat transport in the rotating regime. Indeed, an analysis of the vortex statistics shows that the fraction of the horizontal area that is covered by vortices is aspect-ratio independent when $1/Ro \gg 1/Ro_c$. In agreement with the results of Weiss & Ahlers (2011) we find a vortex-depleted area close to the sidewall. Here, we show that there is also an area with enhanced vortex concentration next to the vortex-depleted edge region and that the absolute widths of both regions are independent of the aspect ratio. This proceeding is a summary of Stevens *et al.* (2011).

1. Introduction

For given aspect-ratio $\Gamma \equiv D/L$ (D is the sample diameter and L its height) the dynamics of a Rayleigh-Bénard system (Ahlers *et al.* (2009)), i.e. fluid between two parallel plates heated from below and cooled from above is determined by the Rayleigh number $Ra = \beta g \Delta L^3/(\kappa\nu)$ and the Prandtl number $Pr = \nu/\kappa$. Here β is the thermal expansion coefficient, g the gravitational acceleration, Δ the temperature difference between the plates, and ν and κ are the kinematic and thermal diffusivity, respectively. In rotating Rayleigh-Bénard convection the system is rotated around a vertical axis at an angular speed Ω. The rotation rate of the system is non-dimensionalized in the form of the Rossby number $Ro = \sqrt{\beta g \Delta/L}/(2\Omega)$, which represents the ratio between buoyancy and the Coriolis force (Stevens *et al.* (2011)).

It has been shown by several authors that three different regimes can be identified in RRB convection (Boubnov & Golitsyn (1990); Zhong *et al.* (2009); Stevens *et al.* (2009); Weiss *et al.*

(2010); Kunnen *et al.* (2010*a*); Zhong & Ahlers (2010); Kunnen *et al.* (2011)). As function of increasing rotation rate one first finds a regime without any heat transport enhancement at all in which the large scale circulation (LSC) is still present (regime I). Zhong & Ahlers (2010) showed that – though the Nusselt number is unchanged in this regime – nonetheless various properties of the LSC do change with increasing rotation in this regime. Here we mention the increase in the temperature amplitude of the LSC, the LSC precession (also observed by Hart *et al.* (2002) and Kunnen *et al.* (2008)), the decrease of the temperature gradient along the sidewall, and the increased frequency of cessations. The start of regime II (moderate rotation) is indicated by the onset of heat transport enhancement due to Ekman pumping as is discussed by Zhong *et al.* (2009), Weiss *et al.* (2010) and Weiss & Ahlers (2011). When the rotation rate is increased in regime II the heat transfer increases further until one arrives at regime III (strong rotation), where the heat transfer starts to decrease. This decrease of the heat transfer in regime III is due to the suppression of the vertical velocity fluctuations (Zhong *et al.* (2009); Zhong & Ahlers (2010); Stevens *et al.* (2010*b*)).

Several experimental (Rossby (1969); Liu & Ecke (1997, 2009); King *et al.* (2009); Zhong *et al.* (2009); Stevens *et al.* (2009); Zhong & Ahlers (2010)) and numerical (Julien *et al.* (1996); Sprague *et al.* (2006); Oresta *et al.* (2007); Kunnen *et al.* (2008, 2010*a*); King *et al.* (2009); Schmitz & Tilgner (2009); Zhong *et al.* (2009); Stevens *et al.* (2009); Schmitz & Tilgner (2010); Stevens *et al.* (2010*b*)) studies on RRB convection have shown that in regime II the heat transport with respect to the non-rotating case increases due to rotation. A detailed overview of the parameter ranges covered in the different experiments can be found in the $Ra - Pr - Ro$ phase diagram shown in figure 1 of Stevens *et al.* (2010*a*) and the $Ra - Ro - \Gamma$ phase diagram shown in figure 1 of Stevens *et al.* (2011). The heat transport enhancement in regime II is caused by Ekman pumping (Rossby (1969); Zhong *et al.* (1993); Julien *et al.* (1996); Vorobieff & Ecke (2002); Kunnen *et al.* (2008); King *et al.* (2009); Zhong *et al.* (2009); Zhong & Ahlers (2010)). Namely, whenever a plume is formed, the converging radial fluid motion at the base of the plume (in the Ekman boundary layer (BL)) starts to swirl cyclonically, resulting in the formation of vertical vortex tubes. The rising plume induces stretching of the vertical vortex tube and hence additional vorticity is created. This leads to enhanced suction of hot fluid out of the local Ekman layer and thus increased heat transport. Corresponding phenomena occur at the upper boundary (Stevens *et al.* (2011)).

Here we present experimental and numerical data on the heat transport. They cover different but overlapping parameter ranges and thus complement each other. The convection apparatus used in the experiments is described in detail by Kunnen *et al.* (2011). All measurements were made at constant imposed Δ and Ω, and fluid properties were evaluated at $T_m = (T_t + T_b)/2$. In the DNS we solved the three-dimensional Navier-Stokes equations within the Boussinesq approximation in a three dimensional cylindrical domain (Verzicco & Orlandi (1996)). The resolution is sufficient to represent the small scales both inside the bulk of turbulence and in the BLs (where the grid-point density has been enhanced) for the parameters employed here. For details we refer to Stevens *et al.* (2011).

Recently, Weiss *et al.* (2010) and Weiss & Ahlers (2011) showed that the rotation rate at which the onset of heat transport enhancement sets in ($1/Ro_c$) increases with decreasing aspect ratio due to finite size effect. This means that the aspect ratio is an important parameter in RRB convection. Here we report on a systematic study of the influence of the aspect ratio on heat transfer (enhancement) for moderate and strong rotation rates, i.e., for $1/Ro \gg 1/Ro_c$. Based on the numerical data we will show that for $1/Ro \gg 1/Ro_c$ the Nusselt number is independent of the aspect ratio, while there are some visible differences for the non-rotating case. The reason for this is that in the non-rotating case there is a global flow organization, which can be influenced by the aspect ratio. In the rotating regime vertically aligned vortices, in which most of the heat transport takes place (Portegies *et al.* (2008); Grooms *et al.* (2010)), form the dominant feature

of the flow. As this is a local effect the heat transport in this regime does not depend on the aspect ratio. In the last part we will analyze the vortex statistics for the different aspect ratios to support that the vortices are indeed a local phenomenon (Stevens *et al.* (2011)).

2. Results

In figure 1 the heat transport for $\Gamma = 0.5$, $\Gamma = 1$, $\Gamma = 4/3$, and $\Gamma = 2$ at $Ra = 2.91 \times 10^8$ is shown. The strong heat transport enhancement for $1/Ro > 1/Ro_c$ is due to Ekman pumping. The figure shows that the heat transport becomes independent of the aspect-ratio once $1/Ro \gg 1/Ro_c$, while there are some visible differences for the non-rotating case. These small differences in the heat transport for different aspect ratios were also found in the numerical study of Bailon-Cuba *et al.* (2010) and in experiments of Funfschilling *et al.* (2005) and Sun *et al.* (2005).

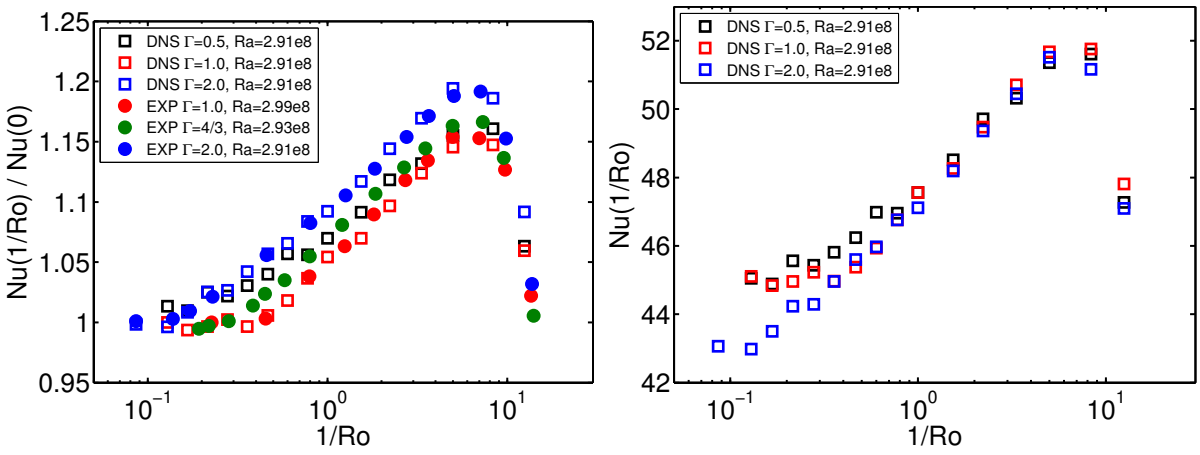

Figure 1. (a) The ratio $Nu(1/Ro)/Nu(0)$ as function of $1/Ro$ for $Ra \approx 3 \times 10^8$ and different Γ. The experimental results for $\Gamma = 1$, $\Gamma = 4/3$, and $\Gamma = 2$ are indicated in red, dark green, and blue solid circles, respectively. The DNS results for $\Gamma = 0.5$, $\Gamma = 1$, and $\Gamma = 2$ are indicated by black, red and blue open squares, respectively. (b) The absolute Nusselt number of the simulation data presented in panel a. The results for $\Gamma = 0.5$, $\Gamma = 1$, and $\Gamma = 2$ are indicated by black, red and blue open squares, respectively. All presented data are for $Pr = 4.38$. Figure taken from Stevens *et al.* (2011) .

For the non-rotating case the flow organizes globally in the large scale convection roll. Because this global flow structure can depend on the aspect-ratio, there can be small variations in the Nusselt number as function of the aspect-ratio. For strong enough rotation, i.e. $1/Ro \gg 1/Ro_c$, the global LSC is replaced by vertically-aligned vortices as the dominant feature of the flow (Kunnen *et al.* (2010*a*); Zhong *et al.* (2009); Stevens *et al.* (2010*b*); Zhong & Ahlers (2010)). In this regime most of the heat transport takes place in vertically-aligned vortices (Portegies *et al.* (2008); Grooms *et al.* (2010)). Because the vortices are a local effect the influence of the aspect-ratio on the heat transport in the system should be negligible (Stevens *et al.* (2011)).

To investigate this idea we made three-dimensional visualizations of the temperature isosurfaces at $Ra = 2.91 \times 10^8$, $Pr = 4.38$, and $1/Ro = 3.33$, for the different aspect ratios, see figure 2. Indeed the figures confirm that vertically-aligned vortices are formed in all aspect-ratio samples. Furthermore, the figure reveals that a larger number of vortices is formed in the $\Gamma = 1$ and $\Gamma = 2$ samples than in the $\Gamma = 0.5$ sample. This is expected, since these samples have a larger horizontal extension (Stevens *et al.* (2011)).

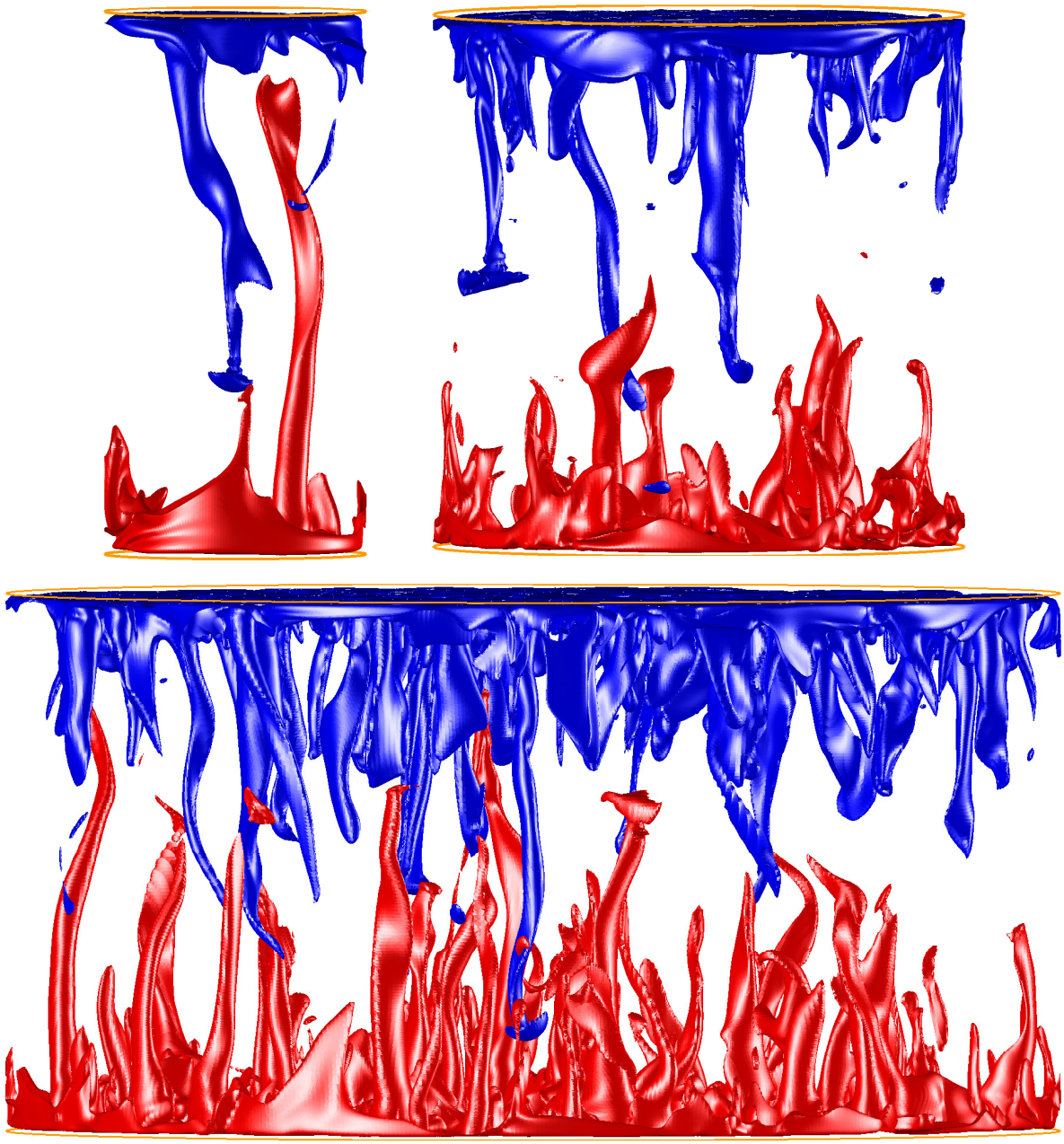

Figure 2. 3D visualization of the temperature isosurfaces in the cylindrical sample at 0.65Δ (red) and 0.35Δ (blue), respectively for $Ra = 2.91 \times 10^8$, $Pr = 4.38$, $1/Ro = 3.33$ and $\Gamma = 0.5$ (left plot), $\Gamma = 1.0$ (middle plot), and $\Gamma = 2.0$ (right plot). Figure taken from Stevens *et al.* (2011).

In order to reveal the structure of the flow in more detail we study the velocity fields at the kinetic BL height near the bottom plate. For this we use the so-called Q-criterion (Boubnov & Golitsyn (1986); Vorobieff & Ecke (2002); Kunnen *et al.* (2010*b*); Weiss *et al.* (2010)). This criterion requires that the quantity Q_{2D} (McWilliams (1984); Stevens *et al.* (2009)), which is a quadratic form of various velocity gradients, is calculated in a plane of fixed height. From a visualization of the vortex distribution, see (Weiss *et al.* (2010)) and (Stevens *et al.* (2011)), we

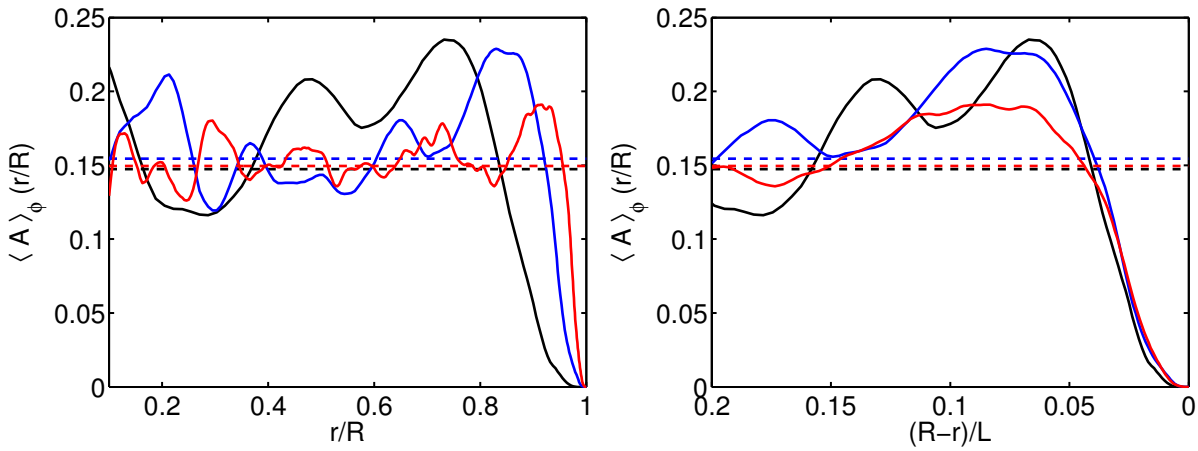

Figure 3. Azimuthal average $\langle A \rangle_{r/R}$ of the vortex density A for $Ra = 2.91 \times 10^8$, $Pr = 4.38$ and $3.33 < 1/Ro < 8.33$ as function of r/R (panel a) and $(R-r)/L$ for different aspect ratios. The solid black, blue, and red lines indicated the distribution for $\Gamma = 0.5$, $\Gamma = 1.0$, and $\Gamma = 2.0$. The dashed lines indicate the average horizontal area covered by vortices. The data for each aspect ratio are based on 12 snapshots. Figure taken from (Stevens *et al.* (2011))

find that the vortices are in general randomly distributed. In addition, we calculated the fraction of the horizontal area that is covered with vortices as function of the radial position. The result is shown in figure 3. Figure 3a confirms that no vortices are formed close to the sidewall, while in the bulk their fraction is roughly constant. Figure 3b shows that the size of the region close to the sidewall where no vortices are formed is roughly independent of the aspect ratio (Stevens *et al.* (2011)).

This is in agreement with the predication of Weiss & Ahlers (2011) that is derived from a phenomenological Ginzburg-Landau model. As detailed information about the flow field is needed to determine the vortex distribution it is very hard to obtain this data from experimental measurements (Kunnen *et al.* (2010*b*)). In figure 3b one can see that the vortex density in the region $(R-r)/L \lesssim 0.015$ decreases faster to zero than for $(R-r)/L \gtrsim 0.015$, which is due to the vortex detection method employed in this study. More specifically, we detect only the core of the vortex. As the vortex core is always formed some distance away from the wall this causes an (artificial) enhanced decrease in the vortex density in the direct vicinity of the wall. The origin of the peaks in the distribution function is similar to the origin of the peaks observed in pair correlation functions of the distribution of hard disks (Stevens *et al.* (2011)).

However, and this is the main point here, one can see in figure 3 that the fraction of the horizontal area that is covered by vortices, see the dashed lines in the figure, is independent of the aspect ratio. This means that the vortices are indeed a local effect. This observation supports our finding that the heat transport is independent of the aspect ratio in the rotating regime. Based on the observation that less vortices are formed close to the sidewalls, one would have expected that the vortex density averaged over the whole area is higher for larger aspect ratio. The reason is that for larger aspect ratio samples this vortex-depleted sidewall region is relatively smaller than for smaller aspect ratio ones. However, just next to the vortex depletion region we find a region where the vortex density is enhanced. As is shown in figure 3b, the absolute width of this region seems to be rather independent of the aspect ratio of the sample, too. Hence the effect of the vortex depletion and the vortex enhancement region on the horizontally averaged vortex density cancel out in first order (Stevens *et al.* (2011)).

3. Discussion

In summary, we investigate the effect of the aspect ratio on the heat transport in turbulent rotating Rayleigh-Bénard convection by results obtained from experiments and direct numerical simulations. We find that the heat transport in the rotating regime is independent of the aspect ratio, although there are some visible differences in the heat transport for the different aspect ratios in the non-rotating regime at $Ra = 2.91 \times 10^8$. This is because in the non-rotating regime the aspect ratio can influence the global flow structure. However, in the rotating regime most heat transport takes place in vertically-aligned vortices, which are a local effect. Based on the simulation results we find that the fraction of the horizontal area that is covered by the vortices is independent of the aspect ratio, confirming that the vertically-aligned vortices are indeed a local effect. This supports the simulation results, which show that the heat transport becomes independent of the aspect ratio in the rotating regime. In addition, it confirms the main assumption that is used in most models, which consider a horizontally periodic domain (Legg *et al.* (2001); Portegies *et al.* (2008); Grooms *et al.* (2010)), that are developed to understand the heat transport in rotating turbulent convection. The analysis of the vortex statistics also revealed that the vortex concentration is reduced close to the sidewall, while the distribution is nearly uniform in the center. In between these two regions, there is a region of enhanced vortex concentration. The widths of both that region and the vortex-depleted region close to the sidewall are independent of the aspect ratio. This analysis highlights the value of numerical simulations in turbulence research: The determination of the vortex distribution requires detailed knowledge of the flow field and therefore it would have been very difficult to obtain this finding purely from experimental measurements (Stevens *et al.* (2011)).

Acknowledgments

We gratefully acknowledge various discussions with Guenter Ahlers over this line of research and his helpful comments on our manuscript. The authors wish to thank Eric de Cocq, Gerald Oerlemans, and Freek van Uittert (design and manufacturing of the experimental set-up) for their contributions to this work, and Jaap van Wensveen of Tempcontrol for advice and helping to calibrate the thermistors. We thank Chao Sun for stimulating discussions. We thank the DEISA Consortium (www.deisa.eu), co-funded through the EU FP7 project RI-222919, for support within the DEISA Extreme Computing Initiative. We thank Wim Rijks (SARA) and Siew Hoon Leong (Cerlane) (LRZ) for support during the DEISA project. The simulations were performed on the Huygens cluster (SARA) and HLRB-II cluster (LRZ). RJAMS was financially supported by the Foundation for Fundamental Research on Matter (FOM).

References

Ahlers, G., Grossmann, S. & Lohse, D. 2009 Heat transfer and large scale dynamics in turbulent Rayleigh-Bénard convection. *Rev. Mod. Phys.* **81**, 503.

Bailon-Cuba, J., Emran, M.S. & Schumacher, J. 2010 Aspect ratio dependence of heat transfer and large-scale flow in turbulent convection. *J. Fluid Mech.* **655**, 152–173.

Boubnov, B. M. & Golitsyn, G. S. 1986 Experimental study of convective structures in rotating fluids. *J. Fluid Mech.* **167**, 503–531.

Boubnov, B. M. & Golitsyn, G. S. 1990 Temperature and velocity field regimes of convective motions in a rotating plane fluid layer. *J. Fluid Mech.* **219**, 215–239.

Funfschilling, D., Brown, E., Nikolaenko, A. & Ahlers, G. 2005 Heat transport by turbulent Rayleigh-Bénard convection in cylindrical cells with aspect ratio one and larger. *J. Fluid Mech.* **536**, 145–154.

Grooms, I., Julien, K., Weiss, J.B. & Knobloch, E. 2010 Model of convective Taylor Columns in rotating Rayleigh-Bénard convection. *Phys. Rev. Lett.* **104**, 224501.

Hart, J. E., Kittelman, S. & Ohlsen, D. R. 2002 Mean flow precession and temperature probability density functions in turbulent rotating convection. *Phys. Fluids* **14**, 955–962.

Julien, K., Legg, S., McWilliams, J. & Werne, J. 1996 Rapidly rotating Rayleigh-Bénard convection. *J. Fluid Mech.* **322**, 243–273.

King, E. M., Stellmach, S., Noir, J., Hansen, U. & Aurnou, J. M. 2009 Boundary layer control of rotating convection systems. *Nature* **457**, 301.

Kunnen, R. P. J., Clercx, H. J. H. & Geurts, B. J. 2008 Breakdown of large-scale circulation in turbulent rotating convection. *Europhys. Lett.* **84**, 24001.

Kunnen, R. P. J., Geurts, B. J. & Clercx, H. J. H. 2010*a* Experimental and numerical investigation of turbulent convection in a rotating cylinder. *J. Fluid Mech.* **82**, 445–476.

Kunnen, R. P. J., Geurts, B. J. & Clercx, H. J. H. 2010*b* Vortex statistics in turbulent rotating convection. *Phys. Rev. E* **82**, 036306.

Kunnen, R. P. J., Stevens, R. J. A. M., Overkamp, J., Sun, C., van Heijst, G.J.F. & Clercx, H.J.H. 2011 The role of Stewartson and Ekman layers in turbulent rotating Rayleigh-Bénard convection. *submitted to J. Fluid. Mech.* .

Legg, S., Julien, K., McWilliams, J. & Werne, J. 2001 Vertical transport by convection plumes: modification by rotation. *Phys. Chem. Earth (B)* **26**, 259–262.

Liu, Y. & Ecke, R. E. 1997 Heat transport scaling in turbulent Rayleigh-Bénard convection: effects of rotation and Prandtl number. *Phys. Rev. Lett.* **79**, 2257–2260.

Liu, Y. & Ecke, R. E. 2009 Heat transport measurements in turbulent rotating Rayleigh-Bénard convection. *Phys. Rev. E* **80**, 036314.

McWilliams, J. C. 1984 The emergence of isolated coherent vortices in turbulent flow. *J. Fluid Mech.* **146**, 21–43.

Oresta, P., Stingano, G. & Verzicco, R. 2007 Transitional regimes and rotation effects in Rayleigh-Bénard convection in a slender cylindrical cell. *Eur. J. Mech.* **26**, 1–14.

Portegies, J. W., Kunnen, R. P. J., van Heijst, G. J. F. & Molenaar, J. 2008 A model for vortical plumes in rotating convection. *Phys. Fluids* **20**, 066602.

Rossby, H. T. 1969 A study of Bénard convection with and without rotation. *J. Fluid Mech.* **36**, 309–335.

Schmitz, S. & Tilgner, A. 2009 Heat transport in rotating convection without Ekman layers. *Phys. Rev. E* **80**, 015305.

Schmitz, S. & Tilgner, A. 2010 Transitions in turbulent rotating Rayleigh-Bénard convection. *Geophysical and Astrophysical Fluid Dynamics* **104**, 481–489.

Sprague, M., Julien, K., Knobloch, E. & Werne, J. 2006 Numerical simulation of an asymptotically reduced system for rotationally constrained convection. *J. Fluid Mech.* **551**, 141–174.

Stevens, R. J. A. M., Clercx, H. J. H. & Lohse, D. 2010*a* Boundary layers in rotating weakly turbulent Rayleigh-Bénard convection. *Phys. Fluids* **22**, 085103.

Stevens, R. J. A. M., Clercx, H. J. H. & Lohse, D. 2010*b* Optimal Prandtl number for heat transfer in rotating Rayleigh-Bénard convection. *New J. Phys.* **12**, 075005.

Stevens, R. J. A. M., Overkamp, J., Lohse, D. & Clercx, H.J.H. 2011 Effect of aspect-ratio on vortex distribution and heat transfer in rotating Rayleigh-Bénard. *submitted to Phys. Rev. E* .

Stevens, R. J. A. M., Zhong, J.-Q., Clercx, H. J. H., Ahlers, G. & Lohse, D. 2009 Transitions between turbulent states in rotating Rayleigh-Bénard convection. *Phys. Rev. Lett.* **103**, 024503.

Sun, C., Xia, K. Q. & Tong, P. 2005 Three-dimensional flow structures and dynamics of turbulent thermal convection in a cylindrical cell. *Phys. Rev. E* **72**, 026302.

Verzicco, R. & Orlandi, P. 1996 A finite-difference scheme for three-dimensional incompressible flow in cylindrical coordinates. *J. Comput. Phys.* **123**, 402–413.

Vorobieff, P. & Ecke, R. E. 2002 Turbulent rotating convection: an experimental study. *J. Fluid Mech.* **458**, 191–218.

Weiss, S. & Ahlers, G. 2011 Heat transport by turbulent rotating Rayleigh-Bénard convection. *submitted to J. Fluid. Mech.* .

Weiss, S., Stevens, R.J.A.M., Zhong, J.-Q., Clercx, H.J.H., Lohse, D. & Ahlers, G. 2010 Finite-size effects lead to supercritical bifurcations in turbulent rotating Rayleigh-Bénard convection. *Phys. Rev. Lett.* **105**, 224501.

Zhong, F., Ecke, R. E. & Steinberg, V. 1993 Rotating Rayleigh-Bénard convection: asymmetrix modes and vortex states. *J. Fluid Mech.* **249**, 135–159.

Zhong, J.-Q. & Ahlers, G. 2010 Heat transport and the large-scale circulation in rotating turbulent Rayleigh-Bénard convection. *J. Fluid Mech.* **665**, 300–333.

Zhong, J.-Q., Stevens, R. J. A. M., Clercx, H. J. H., Verzicco, R., Lohse, D. & Ahlers, G. 2009 Prandtl-, Rayleigh-, and Rossby-number dependence of heat transport in turbulent rotating Rayleigh-Bénard convection. *Phys. Rev. Lett.* **102**, 044502.